PCCP

PAPER

Check for updates

Designing stable binary endohedral fullerene lattices

Abigail Miller, Matthew Halstead, Elena Besley [ID] and Anthony J Stace [ID] *

Nanoparticle lattices and endohedral fullerenes have both been identified as potential building blocks for future electronic, magnetic and optical devices; here it is proposed that it could be possible to combine those concepts and design stable nanoparticle lattices composed from binary collections of endohedral fullerenes. The inclusion of an atom, for example Ca or F, within a fullerene cage is known to be accompanied by a redistribution of surface charge, whereby the cage can acquire either a negative (Ca) or positive (F) charge. From calculations involving a combination of van der Waals and many-body electrostatic interactions, it is predicted that certain binary combinations, for example a metal (A) and a halogen (B), could result in the formation of stable nanoparticle lattices with the familiar AB and AB_2 stoichiometries. Much of the stability is due to Coulomb interactions, however, charge-induced and van der Waals interactions, which always enhance stability, are found to extend the range of charge on a cage over which lattices are stable. Some lattice types are shown to be three or four times more stable than an equivalent neutral C_{60} structure. An extension of the calculations to the fabrication of structures involving endohedral C_{84} is also discussed.

1 Introduction

The fabrication of both nanoparticles[1–3] and molecular fullerenes[4–6] into functional materials has advanced significantly and has now reached a point where some of their unique properties are becoming fully characterised leading to the development of future electronic, magnetic and optical devices. For fullerenes, these advances have come about because of a dramatic increase in the ability of synthetic techniques to prepare a wide range of endohedral fullerenes, $X@C_n$, where n usually starts at 60, and for X as a metal, a significant fraction of the periodic table has been accessed.[4–6] Particular attention has been paid to the encapsulation of rare-earth metals as these may have applications in optics and could form new magnetic and electronic materials.[4–6] For example, $Gd@C_{82}$ has been shown to display gate-controlled switching between electronic states in the presence of an external electric field.[7] Recent work has also demonstrated that other metals, such as encapsulated lithium, $Li@C_{60}$, have the potential to act as molecular switches,[8] and calculations on $Ca@C_{60}$ have identified internal motion on the part of the metal atom as a mechanism for switching charge polarisation on the cage.[9]

Parallel to this work on fullerenes, has been the fabrication of nanoparticle crystals with compositions varying from polymers through semiconductors to metal-centred particles,[1–3]

and where self-assembly frequently leads to the formation of ordered lattices with regular structures resembling those adopted by crystalline atomic materials, *e.g.* NaCl, CsCl, AlB_2 *etc.* Depending on the nature of the particles used in the fabrication process, the lattices have been identified as materials which could have a range of unique properties.[1–3]

The purpose of this work is to use a recent development in the theory of many-body electrostatic interactions[10] to explore some of the known characteristics of endohedral fullerenes with a view to determining if they could form new and novel nanolattice structures. As a consequence, some of the optical and electrical properties previously identified for fullerenes,[7,8] could be incorporated into new materials fabricated into the regular lattice structures known to be adopted by nanoparticles.[1–3]

The literature on nanoparticle lattices[1–3] shows there to be a certain degree of ambiguity in the nature of the constituent particles: they are often charged in isolation, but there is uncertainty as to whether or not any charge remains in the lattice once the particles have assembled. Additionally, there is often some dispersion in particle size; and the particles are frequently decorated with ligands which could influence both van der Waals interactions and the dielectric constant of, for example, a particle that has a metallic core. In contrast, much of this uncertainty disappears with fullerenes, C_n: their exact size is known and shows no dispersion for a fixed value of n;[11] the dielectric constant is known;[12] an accurate van der Waals potential is available;[11,13,14] and finally, whilst the particles are

School of Chemistry, University of Nottingham, University Park, Nottingham, NG7 2RD, UK. E-mail: anthony.stace@nottingham.ac.uk

10044 | *Phys. Chem. Chem. Phys.*, 2022, **24**, 10044–10052

This journal is © the Owner Societies 2022

overall neutral, a charge of either sign can be induced on the cage through the judicious selection of X, the encapsulated species in $X@C_n$.[4–6] Thus, interacting particles will experience a combination of electrostatic and van der Waals interactions that can be fully characterized to define a lattice structure and a lattice energy. Several stable endohedral fullerene complexes involving $Li@C_{60}$ have already been prepared,[15–17] and of these, $Li^+@C_{60}\cdot SbCl_6^-$,[15] and $Li^+@C_{60}\cdot PF_6^-$,[16] are probably the most fully characterised. The stability of such complexes relies on electron transfer between the two constituents leading to the formation of an ionic solid, and attempts to form similar complexes involving other metallofullerenes have not been successful.[6] In part, this problem appears due to the extreme reactivity of $X@C_{60}$ fullerenes;[6] however, samples of crystalline C_{60} metallofullerenes have been prepared through functionalization, which has been shown to increase the HOMO–LUMO gap thereby reducing reactivity.[18] Issues with the reactivity of endohedral C_{60} metallofullerenes would clearly present difficulties with fabricating the types of lattices envisaged here; however, C_{60} is the most fully characterised of the fullerenes and those features of the molecule are used to underpin the calculations.

The ideas discussed here are equally applicable to any quasi-spherical fullerene, such as C_{84}, and recent work on electrostatic interactions between spheroids offers the potential to extend this type of study to ellipsoid structures, such as C_{70}.[19] Calculations with a two-body version of the electrostatic theory have successfully accounted for a range of experimental measurements on the gas phase fragmentation patterns of a series of charged fullerenes.[20]

In the analysis that follows, each endohedral fullerene in the form of $X@C_{60}$ remains overall neutral, but because many of the interactions could involve fractional amounts of charge, it is possible to explore the participation of metallofullerenes that may not be susceptible to reactivity or the donation or acceptance of integer numbers of electrons.

2 Theory

2.1 Many-body electrostatic theory

The lattices to be simulated are represented by collections of non-overlapping charged dielectric spheres that are arranged into one of the selected lattice structures in three-dimensional space. Each particle is centred at a given lattice site, has a radius r_i and a dielectric constant, and they are all suspended in a homogeneous dielectric medium. Each particle carries a free charge q_i, uniformly distributed over the surface and is represented by a density of free charge, $\sigma_{f,i} = q_i/(4\pi r_i^2)$. The presence of free charge on the particles gives rise to an electrical potential from which the electrostatic potential energy can be determined. The electrostatic problem is formulated in terms of set of equations which are solved iteratively to give the total electrostatic energy of the system and the net electrostatic force on each particle is calculated as the gradient of the energy with respect to changes in position.[10] For examples that involve large

numbers of particles, evaluation of the total energy benefits from the implementation of a fast multipole method (FMM), which provides a significant enhancement to the speed of computation, to the point where the computation of the force is scaled lineally with the number of particles.[10]

In the examples given, charge-induced multipolar interactions are considered up to the sixth degree (64 pole), where the non-additive nature of such interaction[10] is taken into account through the mutual polarisation of charged, dielectric particles. The accuracy of each calculation is controlled through a maximum number of real spherical harmonics utilised in discretisation of the model and has been set at 6 in all calculations reported here, which as convergence tests show, equates to an average error of 4% in the multipole terms.[21] The results given below were typically taken from calculations on up to 5000 particles.

2.2 van der Waals interactions and partial charge analysis

The van der Waals interactions between C_{60} fullerene molecules were described using two- and three-body potentials given by Pacheco and Prates-Ramalho (PPR).[11] For C_{84} fullerenes, a two-body van der Waals potential due to Girifalco has been used[22] together with parameters taken from Micali et al.,[23] which are summarised in Table 1.

Density functional theory was used to optimise the geometry of endohedral fullerenes using the wB97X-D/6-311G* level of theory, as provided by the Q-Chem 5.0 quantum chemistry software package.[24] For the prediction of partial charges, the density-derived electrostatic and chemical (DDEC) method[25–27] has been selected as it reproduces reference ion states and provides an approximately spherical atomic electron distribution, thus combining the advantages of both the Hirshfeld[28] and iterative stockholder atom[29] methods.

3 Analysis of lattice types

The energetics of lattices consisting of two frequently observed binary nanoparticle stoichiometries,[1–3] AB and AB_2, has been explored as a function of the ratio of charge residing on cages associated with separate A and B endohedral $X@C_{60}$ fullerenes (how charge appears on the fullerenes is the subject of a detailed discussion below). The total interaction energy of each

Table 1 Parameters used to describe van der Waals interactions: PPR potential[11] for C_{60}, and the Girifalco Potential[23] for C_{84}

C_{60}	Parameters
Radius	0.5025 nm
Dielectric Constant	3.46

C_{84}	Parameters
d	0.8401 nm
α	5.356×10^{-14} erg
β	3.542×10^{-10} erg
R_0	1.1357 nm
$-\varepsilon/K_B$	4081.5 K
Dielectric constant	4.24

This journal is © the Owner Societies 2022

Phys. Chem. Chem. Phys., 2022, **24**, 10044–10052 | **10045**

lattice type has been determined from calculations on a combination of van der Waals (vdW), Coulomb and charge induced multipolar interactions. The vdW interactions are described following the work of Doye, Wales and co-workers,[13,14] who have demonstrated that expressions due to Pacheco and Prates-Ramalho[11] can be used to determine minimum energy structures for large clusters of C_{60} molecules. The electrostatic contributions to the stability of collections of endohedral fullerene cages have been calculated using a recently developed theory of many-body electrostatic interactions,[10] which provides quantitatively accurate descriptions of the large number of Coulomb and charge-induced multipole interactions that may be present in an ordered lattice of charged particles. Batista *et al.*[30] have previously recognised the significance of nonadditive interactions in the treatment of nanoparticle structures.

Fig. 1 shows small sections of each of the lattice types examined. In addition to the obvious colour difference between negatively and positively charged particles, there are also regions of more intense colour showing enhanced charge due to polarisation. This is particularly evident in, for example, structure (1b) where there is a large contribution from charge-induced polarisation (illustrated in the expanded image and see Fig. 2(b) below). Also evident in some of the AB_2 structures, for example, (1d) and (1e), is the presence in of negative charge (shown in blue) between two adjacent positively charged particles (shown as red). This latter effect is highlighted in the
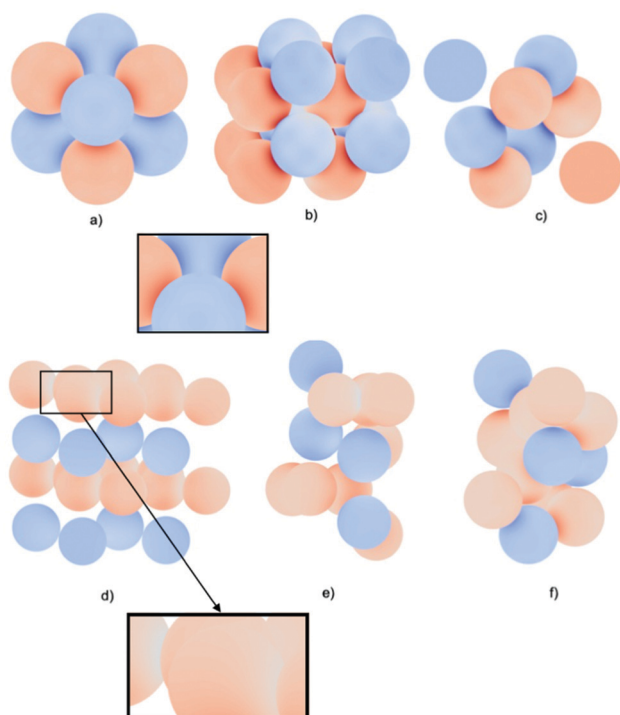

Fig. 1 Section of each lattice type: (a) NaCl; (b) CsCl; (c) ZnS; (d) AlB_2; (e) $MgZn_2$; (f) $SeAg_2$. Shading on each particle depicts the calculated surface charge as being either negative (blue) or positive (red). Regions of more intense colouration correspond to enhanced charge due to the polarisation of bound charge and are shown in the enlarged images.

expanded image and has been discussed previously,[31,32] where it has been shown that such mutual polarisation can ultimately lead to like-charge attraction.

Calculation of the many-body electrostatic energy takes as their input the number of particles, each with an assigned radius, dielectric constant (relative permittivity), charge and position on a three-dimensional lattice.[10,21] Output consists of the distribution of surface charge and the electrostatic energy (or force) of an assembly of particles.[10] The charge that is assigned to each particle, denoted here as free charge, is the quantity over which experimentalists generally have control, for example through solvent or ionic strength, and is treated in the model as being uniformly distributed over the surface of each particle. However, the particles become polarised in the presence of an external electric field, which in this context is generated by free charge on adjacent particles. Polarised bound charge accumulates on the surface of each particle, which leads to an anisotropic distribution of total (free + bound) surface charge. This is coupled with similar effects on all other particles *via* mutual polarisation; a mechanism which can only be properly described through a many-body formalism.[10] By separately evaluating the significance of vdW, Coulomb and charge-induced interactions, it is possible to characterise a given lattice type in terms of the properties of constituent $X@C_{60}$ molecules that are responsible for stability.

The formation of a binary lattice requires there to be two types of particle, which is not immediately obvious in the case of fullerenes; however, calculations show that changes in the nature of the encapsulated species can utilise electron affinity to create a positive or negative charge on the former. Table 2 summarises the results of calculations showing the consequences of introducing different atoms into the C_{60} cage.[33–36] The presence of a metal atom, such as calcium or lithium, generally has the effect of ionising the atom and at the same time adding electron density to the cage, and resident metals and metal complexes have been classified as being either mono, di, or trivalent[4–6] depending on the number of electrons assumed to be transferred to the cage.

The wide range of metal atoms that have been (or could be) encapsulated in fullerenes means that, for the examples shown in Table 2, the calculated charge on the cage can vary between $-0.1\ e$ and $-2.0\ e$.[33–36] In contrast, the introduction of a fluorine or chlorine atom removes electron density from the cage and adds negative charge to the endohedral F or Cl atom.[33] Since chlorine has the higher atomic electron affinity, the calculated charge on a cage induced by its presence is an upper limit to what can be achieved with a single atom. Experimental confirmation of the anticipated charge transfer when metal atoms are encapsulated in fullerenes, can be seen from studies of $Li@C_{60}$,[37,38] where it has been shown that in isolation, $Li@C_{60}$ takes the form $Li^+C@_{60}^{\bullet-}$. However, in the condensed phase, the endohedral complex has been shown to form a dimer $Li@C_{60}$–$Li@C_{60}$.[37,38]

The limitations discussed above regarding the amount of positive or negative charge that can be transferred to a fullerene cage could be relaxed with the inclusion of species more
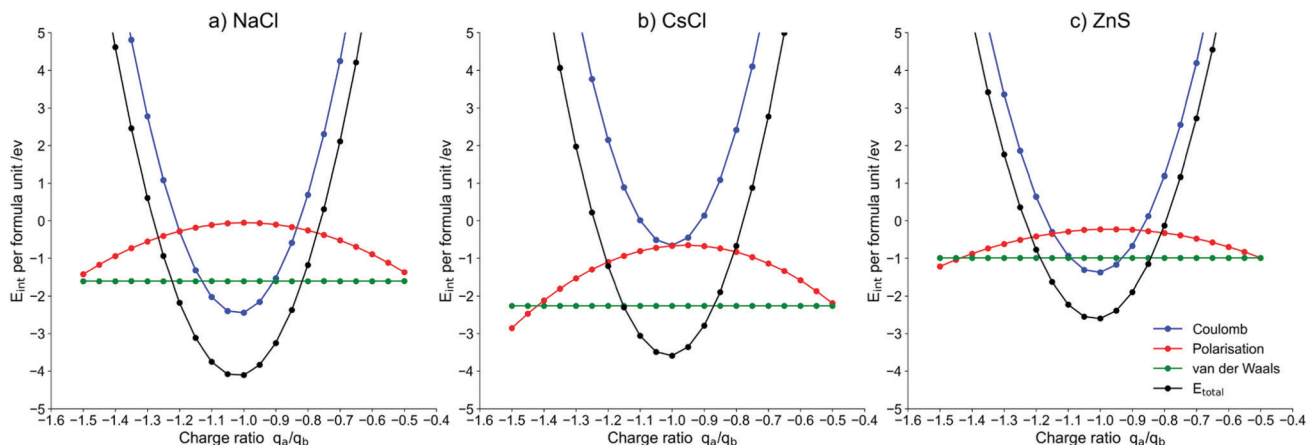
Fig. 2 Individual contributions to the total energy per formula unit for lattice structures of the type (left to right): NaCl; CsCl; and ZnS, each consisting of equal numbers of positively and negatively charged $X@C_{60}$ fullerene cages.

complex than simple atoms. The presence of both Sc_3N and Ti_3C_3 in a fullerene are thought to result in the transfer of up to 6 electrons to the cage;[39,40] likewise, recent calculations have shown that a series of superhalogens, including AlF_4, MgF_3 and LiF_2,[41] together with $PtCl_9$ and Pt_2Cl_9,[42] and Mg_3F_7[43] all have electron affinities higher than that of chlorine, and in some cases, calculations have already shown these molecules to be capable of removing electron density from the C_{60} cage.[39,41]

Finally, experiment and theory have identified molecules capable of forming stable dianions with first and second electron affinities above that of the single electron affinity of chlorine. These species include ZrF_6[44] and $B_{12}(CN)_{12}$,[45–47] which can form stable dianions when the second electron becomes trapped behind a Coulomb barrier; as such, their inclusion in an endohedral fullerene, could result in the cage losing up to 2 electrons and acquiring a charge of +2. Many of these molecular examples would obviously require accommodation in fullerenes larger than C_{60};[48] however, they do offer the possibility for generating a wider range of lattice structures.

A large number of metal-containing endohedral fullerenes that have, to date, been synthesized are readily available.[4–6] What is less obvious are routes to the synthesis of the required

Table 2 Summary of calculated charge populations on the C_{60} cage following the encapsulation of metal and halogen atoms. The numbers quoted are dependent on the methods used to calculate the populations, details of which can be found in the cited articles. Values in bold indicate results produced in this work

Endohedral species	Calculated charge on the cage (e)
Mg	-0.10[34]
Na	-0.88[34]
K	-0.95[34]
Al	-0.89[34]
La	-1.07[34]
Lr	-0.77[35]
Au–Au_6	-0.1 to -2.0[36]
Ca	-1.27[34]; -1.33; **-1.44**
Li	-0.68[33]; -0.91[34]; -0.55[35]; **-0.94**
F	0.4[33]; **0.38**
Cl	**0.58**

counter ion, and although recent experiments have identified the formation of stable $F@C_{60}$,[49] that aspect of the work will require further experimental investigation. It is encouraging to note, however, that thermally stable quantities of the non-metallic endohedral fullerenes $N@C_{60}$ and $P@C_{60}$ have been prepared, although calculations show there to be no electron transfer from or to the cage.[50] What all of the examples given in Table 2 do demonstrate, is that there is some flexibility in the amount of charge, either negative or positive, that could be induced to reside on the surface of a fullerene cage. For the purposes of the theory, it is assumed that in all of the examples discussed below the cage has a uniform distribution of charge; this in turn implies that X in $X@C_{60}$ resides at the centre of the cage, which is not always necessarily the case.[4–6,15–17,33–36]

4 Case studies and discussion

The method described is general and is demonstrated in the case studies discussed below.

4.1 $X@C_{60}$ lattice structures

In principle each AB pair should experience three separate electrostatic interactions, which are: (i) the charged core of A interacting with the charged core of B; (ii) an interaction between the charged cores and the charged cages; and (iii) an interaction between the charged cage of A and the charged cage of B. However, a range of experimental and theoretical studies have shown that fullerene molecules act as Faraday cages,[51–58] which means that entities (other cores and cages) external to a given cage are shielded from any charge contained within the cage, i.e. the metal or halogen core. Therefore, electrostatic interactions in AB and AB_2 systems will be dominated by iii, namely interactions between the charges on each A and B cage. Thus, each lattice with, for example, an AB pair in the form of $A@C_{60}^{q+} \cdot B@C_{60}^{q-}$, is treated as a collection of charged, dielectric spheres, for which theory is very well established.[10,31] Experiments on multiply-charged clusters, $(C_{60})_n^{q+}$[59], would suggest that a single-component $X@C_{60}$ nanolattice, where

This journal is © the Owner Societies 2022

Phys. Chem. Chem. Phys., 2022, **24**, 10044–10052 | **10047**

each endootal fullerene cage carries a charge of the same sign will not be stable, but that a lattice of the form $(X@C_{60})_n(C_{60})_m$ which is interspersed with non-endohedral fullerenes with $m > n$ might be.

Two lattice stoichiometries have been the subject of this study, and these are AB and AB_2. For AB systems the calculations discussed below have focussed on nominal charges of $q_A = -1\ e$ and $q_B = +1\ e$ on the cage, but with the negative charge allowed to vary by $\pm 0.5\ e$; thus, reflecting the fact that an exact equal and opposite match of charge on the cages will probably not be possible. For AB_2 systems the nominal charges are $q_A = -2\ e$ and $q_B = +1\ e$, but with a negative charge variation of $\pm 1.0\ e$. For AB combinations where the absolute charge on each cage is different to what is considered here, the Coulomb energies quoted below can be scaled using the product $q_A q_B$.[60] It should again be emphasised that each $X@C_{60}$ and each final nanolattice remains charge neutral. An example of a potential lattice would be an AB structure consisting of unit cells containing $K@C_{60}$ paired with $Cl@C_{60}$.

Results are presented following calculations on two stoichiometries, AB and AB_2, where lattice stabilities have been calculated as a function of the charge ratios q_A/q_B and $q_A/2q_B$, respectively. The intention here is to explore a range of lattice types to see which might be best suited to form a stable crystalline structure. For AB structures, initial calculations were undertaken on the rock salt cubic lattice, which experiment has identified as stable for both pure C_{60} above 249 K[61] and for endohedral fullerenes of the form $Li^+@C_{60}(Y)$, where Y is PF_6^- or ClO_4[15, 16, 17] (although Table 3 shows the cage in $Li@C_{60}$ is calculated to be negatively charged,[33–35] the cage in $Li^+ @C_{60}$ is predicted to carry a charge of $+0.1\ e$[34]). Fig. 2a shows the results of calculations on a lattice composed of negatively and positively charged C_{60} cages arranged in the form of an NaCl face-centered cubic (fcc) crystal. What is immediately obvious from the calculated total energy is that this lattice is very stable over a wide range in the charge ratio, with each of the separate interactions making a contribution to overall stability. For this example, the dominant interactions are Coulomb and van der Waals, with the latter remaining constant across the charge ratio range as it is not sensitive to charge. Where the vdW interaction becomes particularly significant for stabilising the lattice is at those charge ratios where the Coulomb energy becomes positive; also, at these ratios, the contribution from charge-induced interactions, which although small, is always

negative and therefore helps to extend the range of charge over which the lattice remains stable.

Fig. 2b shows the result of calculations on an CsCl body-centered cubic lattice composed of $X@C_{60}$ molecules. Across the charge ratio shown, the lattice is almost as stable as that seen for the fcc lattice; however, in contrast to the fcc lattice, the Coulomb contribution is comparatively small and it is the van der Waals and charge-induced interactions that make significant contributions to overall stability. What is significant for both lattice types is that stability is not restricted to charge ratios close to one; thus, allowing mis-matches of the type seen in Table 2 to still result in a stable lattice. Finally, for the AB lattices, Fig. 1c shows results for a ZnS lattice, which at charge ratios close to 1, has dominant contributions from Coulomb and vdW interactions, but is less stable than the other two lattice types.

Fig. 3a–c show the results of calculations on three AB_2 lattice types, namely, AlB_2 $MgZn_2$ and Ag_2Se. For the AlB_2 lattice, there is very little stability to be gained from Coulomb interactions away from $q_A/q2_B \sim 1$, and it is only the presence of vdW and polarisation interactions that extend stability over what is still a narrow range of charge ratios. In contrast, the stabilities of both the $MgZn_2$ and Ag_2Se fullerene lattices rely almost entirely on Coulomb interactions, which, again, over a very narrow charge ratio, renders both lattices to be far more stable than any of those examined thus far.

Table 3 summarises data on the charge range over which each of the lattice types is calculated to be stable, which given that exact equal and opposite charges on the $X@C_{60}$ constituents of a lattice may not be possible, increases the opportunity to form a stable structure. Taking as a guide to stability, existing data on the neutral C_{60} fcc lattice, where just vdW interactions are present, then a CsCl lattice could be 1.5 to 2 times more stable than its neutral counterpart. However, if it becomes possible to closely match the positively and negatively charged components, then a $SeAg_2$-type lattice looks to be extremely stable.

Fig. 4 summarises the contribution the three separate interactions, Coulomb, charge-induced, and vdW make to the overall stability of each lattice type when the charge ratio, q_A/q_B, is one. There does not appear to be a unique prescription for creating a lattice that is both strongly bound and stable across a wide charge ratio. In three examples, a large Coulomb contribution gives a lattice that, within its class, is strongly

Table 3 Total interaction energies (in eV per unit formula) for endohedral fullerenes arranged in the lattice types NaCl, CsCl, ZnS, AlB_2, $MgZn_2$, $SeAg_2$ at charge ratios between −0.5 and −15

q_A/q_B	−1.5	−1.4	−1.3	−1.2	−1.1	−1.0	−0.9	−0.8	−0.7	−0.6	−0.5
System	Interaction energies in eV per formula unit										
NaCl	9.83	4.61	0.61	−2.18	−3.75	−4.11	−3.25	−1.18	2.11	6.11	12.33
CsCl	12.30	6.47	1.97	−1.21	−3.06	−3.59	−2.79	−0.67	2.77	7.54	13.63
ZnS	10.04	5.36	1.76	−0.77	−2.23	−2.60	−1.90	−0.13	2.72	6.65	12.54
AlB_2	31.15	18.78	9.23	2.50	−1.41	−2.49	−0.76	3.79	11.17	21.37	34.38
$MgZn_2$	40.83	23.06	9.37	−0.22	−5.72	−7.12	−4.44	2.34	13.21	28.17	47.22
$SeAg_2$	40.77	22.68	8.71	−1.16	−6.91	−8.55	−6.08	0.50	11.19	25.99	44.90

10048 | *Phys. Chem. Chem. Phys.*, 2022, **24**, 10044–10052
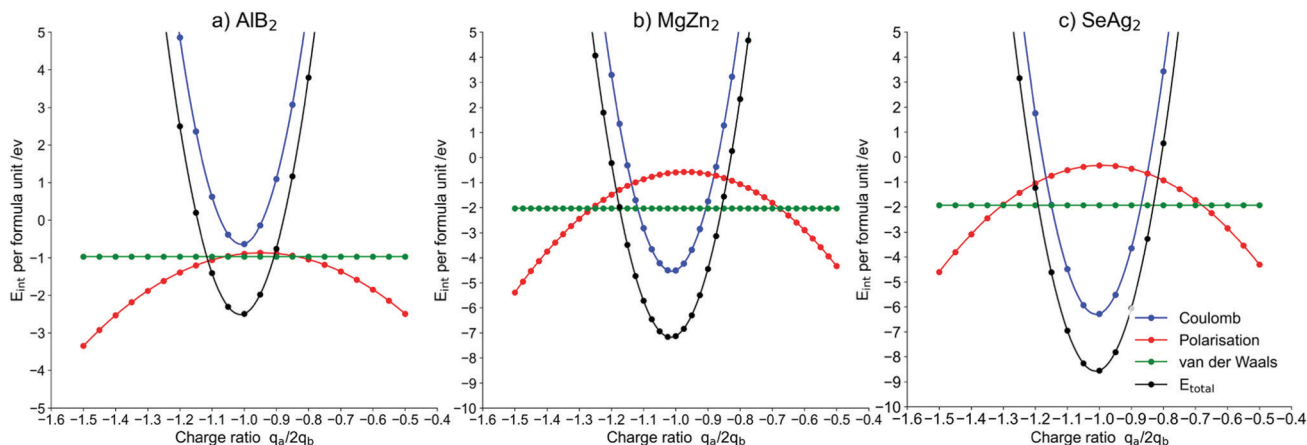
This journal is © the Owner Societies 2022

Fig. 3 Energy per formula unit for lattice structures of the type (from left to right): AlB_2; $MgZn_2$; and $SeAg_2$, each consisting of two positively and one negatively charged $X@C_{60}$ fullerene cage.
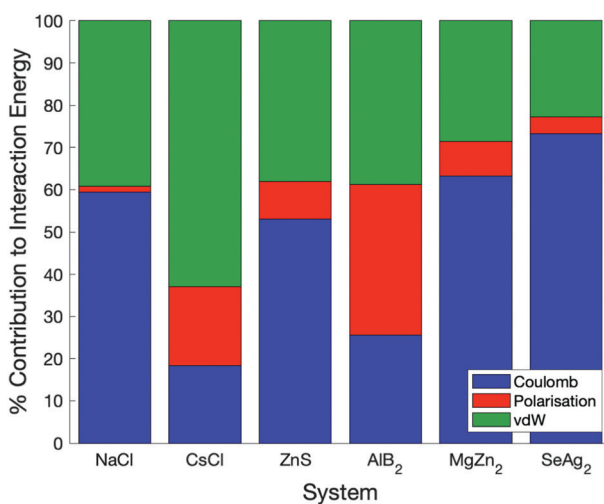

Fig. 4 For each AB and AB_2 lattice type where the charge ratio is one, the percentage contribution to the total energy is shown for each of the following interactions: Coulombic (blue); charge-induced (red); and vdW (green).

Fig. 5 Variation in the stability of NaCl and CsCl lattice types for the situation where $q_A = q_B$, and the charge q on each cage is increased from 0 to 2. The various interactions are shown as follows: van der Waals – dashed lines; polarization – dot-dashed lines; Coulomb – dotted lines; total energy – solid lines. For CsCl the contributions from Coulomb and polarization interactions are almost identical.

bound, but at the same time, vdW and charge-induced interactions could have a significant role in the fabrication of a stable endohedral fullerene lattice. The total energies calculated for all the AB and AB_2 structures are very clearly $\gg kT$, which means that they should remain stable at room temperature and most likely under the operating conditions of any application.

Since there is the potential for generating endohedral fullerenes with charges outside the range considered above for AB structures, two further calculations have been undertaken. Fig. 5 examines how, for the situation where $q_A = -q_B$ in $X@C_{60}$, the stability of NaCl and CsCl lattices varies as the charge q on each cage increase from 0 to 2. As can be seen, the stability of both lattice types increases significantly beyond $q = 1.0$; however, there is also an interesting switch in stability at $q \sim 0.7$ between the fcc lattice of NaCl and the cubic lattice of CsCl, which clearly arises when the large contribution from van der Waals and charge-induced interactions to the stability
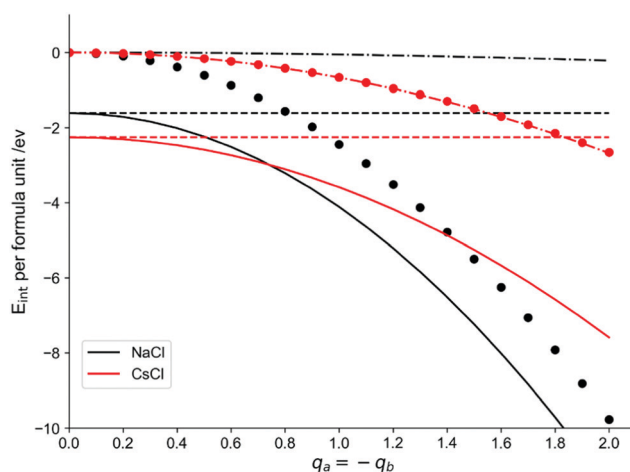
of the CsCl lattice is superseded by the higher Coulomb contribution to the NaCl lattice that varies as q^2 and can be seen in Fig. 1a and 4. The fact that fractional charges, $<1\,e$, on a pair of endohedral fullerenes in an AB structure will form a stable lattice, could help to reduce the possibility of reactivity.[6] The calculated results given in Fig. 5 predict that at zero charge on the particles, the CsCl bcc lattice structure should be more stable than that of the NaCl fcc lattice. If the bcc lattice could be viewed as two interlocking simple cubic lattices, then this result would be consistent with the simple cubic structure observed for pure C_{60} at low temperatures.[61]

4.2 $X@C_{84}$ lattice structures

The availability of a suitable van der Waals potential for C_{84} has made it possible to extend the above calculations to explore the

This journal is © the Owner Societies 2022

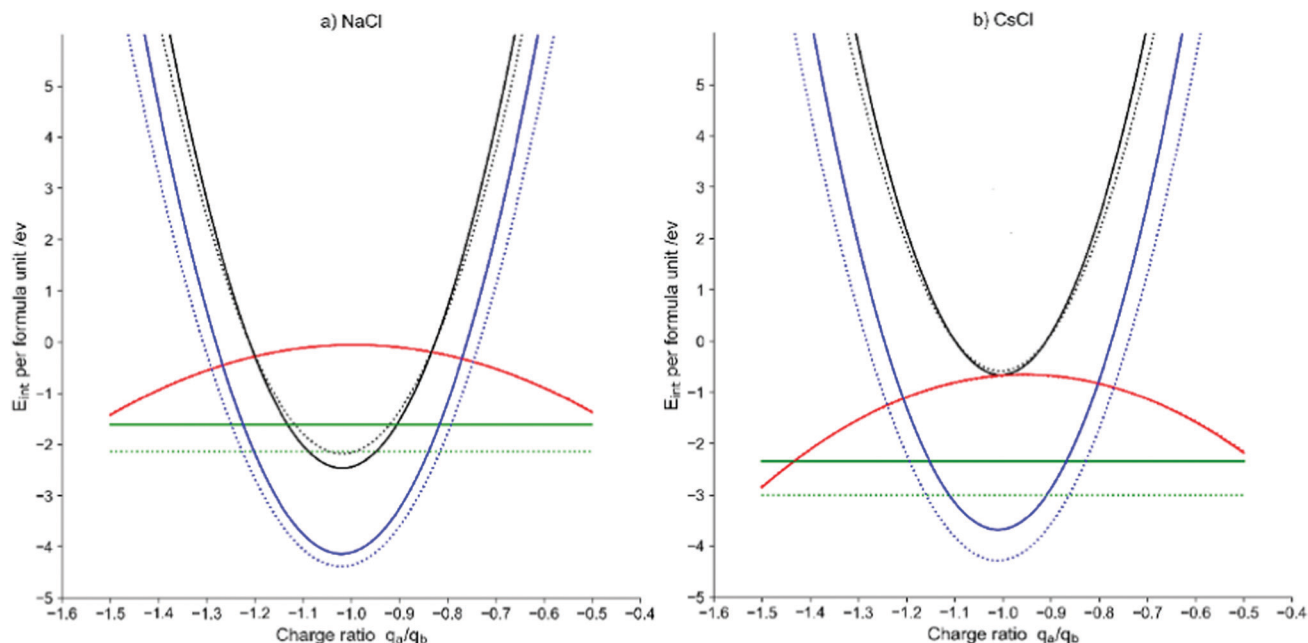*Phys. Chem. Chem. Phys.*, 2022, **24**, 10044–10052 | **10049**

Fig. 6 Comparison between the stabilities of lattice structures composed of $X@C_{60}$ and $X@C_{84}$ fullerene cages. Individual contributions to the total energy per formula unit for lattice structures of the type: (a) NaCl and (b) CsCl, each consisting of equal numbers of positively and negatively charged $X@C_n$ fullerene cages. The solid lines are for C_{60} and the dashed lines C_{84}. Coulomb interactions are shown in black, many-body polarisation interactions in red, and vdW interactions in green. The total interaction energies a shown as blue. For C_{60} the vdW contribution has been calculated using the PPR potential[11], and for C_{84} the Girifalco potential has been used.[22,23]

consequences of utilising larger fullerenes, which would then allow the accommodation of many of the more complex species discussed above. However, there is the possibility that the inclusion of species other than atoms may change the shape of the fullerene cage.[48] For the purposes of these calculations on C_{84}, the van der Waals potential constructed by Girifalco[22] has been used together with the many-body electrostatic theory discussed above. There are a number of parameter sets available for the C_{84} Girifalco potential,[23] and those chosen for these calculations are given in Table 1. In addition, the dielectric constant has been increased from 3.46 used for C_{60} to 4.24.[62] Fig. 6 shows the results, where the individual contributions to total lattice stability are compared for $X@C_{60}$ and $X@C_{84}$. For the individual lattice types, NaCl and CsCl, there are competing contributions to the relative stability. The slightly larger size of C_{84} will lower surface charge density, which, in turn, will reduce both the Coulomb (most noticeable for the NaCl lattice) and polarisation interactions; however, the larger sphere will also be more polarisable. As can be seen from Fig. 6, changes to the electrostatic interactions are marginal, with $X@C_{60}$ appearing as the more stable; however, it is mainly through the van der Waals interaction that $X@C_{84}$ acquires additional stability and for a CsCl lattice type this amounts to ~ 0.5 eV.

5 Conclusions

The proposal is that nanoparticle structures could be fabricated from combinations of appropriate endohedral fullerenes that are capable of forming stable lattices. From the results of

calculations present here, it has been shown that stability is derived, in part, from electrostatic interactions between fullerenes, where the presence of certain endohedral atoms can induce either a negative or positive charge to reside on the cage. For AB and AB_2 structures, varying combinations of Coulomb, charge-induced and van der Waals interactions contribute to overall stability, and because the latter two interactions always enhance stability, their presence has been shown to extend the range of charges over which lattices are stable. The proposed lattice structures differ from those previously identified by experiment for $Li@C_{60}$, in that their formation does not require electron transfer to a counter anion.[15–17] In addition to applications in the form of devices, recent calculations have also shown that arrays of $M@C_{60}$ (M = Na, K, Rb, Cs, Sc, Ti, Mn, Fe) could act as catalysts for the activation of hydrogen,[63] and that embedded metal clusters in the form $M_n@C_{60}$ (M = Mn, Co, Ni, Cu; n = 2–5) could stimulate the oxygen reduction reaction.[64] Both these processes are promoted by the presence of a negative charge on the fullerene cage, and since arrays of these materials alone might not be stable, the results presented above may offer a route to their fabrication.

Conflicts of interest

There are no conflicts to declare.

Acknowledgements

10050 | *Phys. Chem. Chem. Phys.*, 2022, **24**, 10044–10052

This journal is © the Owner Societies 2022

Notes and references

1 M. A. Boles, M. Engel and D. V. Talapin, *Chem. Rev.*, 2016, **116**, 11220–11289.

2 R. Tan, H. Zhu, C. Cao and O. Chen, *Nanoscale*, 2016, **8**, 9944–9961.

3 A. M. Kalsin, M. Fialkowski, M. Paszewski, S. K. Smoukov, K. J. M. Bishop and B. A. Grzybowski, *Science*, 2006, **312**, 420–424.

4 X. Lu, L. Feng, T. Akasaka and S. Nagase, *Chem. Soc. Rev.*, 2012, **41**, 7723–7760.

5 A. A. Popov, S. Yang and L. Dunsch, *Chem. Rev.*, 2013, **113**, 5989–6113.

6 N. Shinohara and H. Tagmatarchis, *Endohedral Metallofullerenes–Fullerenes with Metal Inside*, Wiley, 2015.

7 K. Zhang, C. Wang, M. Zhang, Z. Bai, F.-F. Xie, Y.-Z. Tan, Y. Guo, K.-J. Hu, L. Cao, S. Zhang, X. Tu, D. Pan, L. Kang, J. Chen, P. Wu, X. Wang, J. Wang, J. Liu, Y. Song, G. Wang, F. Song, W. Ji, S.-Y. Xie, S.-F. Shi, M. A. Reed and B. Wang, *Nat. Nanotechnol.*, 2020, **15**, 1019–1024.

8 H. J. Chandler, M. Stefanou, E. E. B. Campbell and R. Schaub, *Nat. Commun.*, 2019, **10**, 2283.

9 G. Raggi, A. J. Stace and E. Bichoutskaia, *Phys. Chem. Chem. Phys.*, 2014, **16**, 23869–23873.

10 E. B. Lindgren, A. J. Stace, E. Polack, Y. Maday, B. Stamm and E. Besley, *J. Comput. Phys.*, 2018, **371**, 712–731.

11 J. M. Pacheco and J. P. Prates Ramalho, *Phys. Rev. Lett.*, 1997, **79**, 3873–3876.

12 C. R. Snyder and J. F. Douglas, *J. Phys. Chem. B*, 2000, **104**, 11058–11065.

13 J. P. Doye and D. J. Wales, *Chem. Phys. Lett.*, 1996, **262**, 167–174.

14 J. P. K. Doye, D. J. Wales, W. Branz and F. Calvo, *Phys. Rev. B: Condens. Matter Mater. Phys.*, 2001, **64**, 235409.

15 S. Aoyagi, E. Nishibori, H. Sawa, K. Sugimoto, M. Takata, Y. Miyata, R. Kitaura, H. Shinohara, H. Okada, T. Sakai, Y. Ono, K. Kawachi, K. Yokoo, S. Ono, K. Omote, Y. Kasama, S. Ishikawa, T. Komuro and H. Tobita, *Nat. Chem.*, 2010, **2**, 678–683.

16 S. Aoyagi, Y. Sado, E. Nishibori, H. Sawa, H. Okada, H. Tobita, Y. Kasama, R. Kitaura and H. Shinohara, *Angew. Chem., Int. Ed.*, 2012, **51**, 3377–3381.

17 S. Aoyagi, K. Miwa, H. Ueno, H. Okada, Y. Matsuo and K. Kokubo, *R. Soc. Open Sci.*, 2018, **5**, 180337.

18 A. Nakagawa, M. Nishino, H. Niwa, K. Ishino, Z. Wang, H. Omachi, K. Furukawa, T. Yamaguchi, T. Kato, S. Bandow, J. Rio, C. Ewels, S. Aoyagi and H. Shinohara, *Nat. Commun.*, 2018, **9**, 3073.

19 I. N. Derbenev, A. V. Filippov, A. J. Stace and E. Besley, *J. Chem. Phys.*, 2020, **152**, 024121.

20 A. Stace and E. Besley, *Phys. Chem. Chem. Phys.*, 2011, **13**, 18339–18346.

21 E. B. Lindgren, B. Stamm, Y. Maday, E. Besley and A. J. Stace, *Philos. Trans. R. Soc., A*, 2018, **376**, 20170143.

22 L. A. Girifalco, *J. Phys. Chem.*, 1992, **96**, 858–861.

23 F. Micali, M. Abramo and C. Caccamo, *J. Phys. Chem. Solids*, 2003, **64**, 319–324.

24 Y. Shao, *Mol. Phys.*, 2015, **113**, 184–215.

25 T. A. Manz and N. G. Limas, *RSC Adv.*, 2016, **6**, 47771–47801.

26 T. A. Manz and D. S. Sholl, *J. Chem. Theory Comput.*, 2010, **6**, 2455–2468.

27 T. A. Manz and D. S. Sholl, *J. Chem. Theory Comput.*, 2012, **8**, 2844–2867.

28 F. L. Hirshfeld, *Theor. Chim. Acta*, 1977, **44**, 129–138.

29 R. J. Lillestolen and T. C. Wheatley, *Chem. Commun.*, 2008, 5909–5911.

30 C. A. S. Batista, R. G. Larson and N. A. Kotov, *Science*, 2015, **350**, 1242477.

31 E. Bichoutskaia, A. L. Boatwright, A. Khachatourian and A. J. Stace, *J. Chem. Phys.*, 2010, **133**, 024105.

32 A. J. Stace, A. L. Boatwright, A. Khachatourian and E. Bichoutskaia, *J. Colloid Interface Sci.*, 2011, **354**, 417–420.

33 A. K. Srivastava, S. K. Pandey, A. K. Pandey and N. Misra, *Aust. J. Chem.*, 2018, **71**, 953–956.

34 E. Broclawik and A. Eilmes, *J. Chem. Phys.*, 1998, **108**, 3498–3503.

35 A. K. Srivastava, S. Pandey and N. Misra, *Mater. Chem. Phys.*, 2016, **177**, 437–441.

36 C. Du, K. Jin and X. Liu, *J. Mater. Sci.*, 2020, **55**, 12980–12994.

37 H. Ueno, S. Aoyagi, Y. Yamazaki, K. Ohkubo, N. Ikuma, H. Okada, T. Kato, Y. Matsuo, S. Fukuzumi and K. Kokubo, *Chem. Sci.*, 2016, **7**, 5770–5774.

38 H. Okada, H. Ueno, Y. Takabayashi, T. Nakagawa, M. VrankićŽć, J. Arvanitidis, T. Kusamoto, K. Prassides and Y. Matsuo, *Carbon*, 2019, **153**, 467–471.

39 S. Stevenson, G. Rice, T. Glass, K. Harich, F. Cromer, M. R. Jordan, J. Craft, E. Hadju, R. Bible, M. M. Olmstead, K. Maitra, A. J. Fisher, A. L. Balch and H. C. Dorn, *Nature*, 1999, **401**, 55–57.

40 D. Hao, L. Yang, B. Li, Q. Hou, L. Li and P. Jin, *J. Phys. Chem. A*, 2020, **124**, 2694–2699.

41 C. Sikorska, *Phys. Chem. Chem. Phys.*, 2016, **18**, 18739–18749.

42 Y. Shi, S. Bian, Y. Ma, Y. Wang, J. Ren and X. Kong, *J. Phys. Chem. A*, 2019, **123**, 187–193.

43 C. Sikorska, *Int. J. Quantum Chem.*, 2018, **118**, e25728.

44 X.-B. Wang and L.-S. Wang, *J. Phys. Chem. A*, 2000, **104**, 4429–4432.

45 S. Giri, B. Z. Child, J. Zhou and P. Jena, *RSC Adv.*, 2015, **5**, 44003–44008.

46 G. Chen, T. Zhao, Q. Wang and P. Jena, *J. Phys. Chem. A*, 2019, **123**, 5753–5761.

47 P. Jena and Q. Sun, *Chem. Rev.*, 2018, **118**, 5755–5870.

This journal is © the Owner Societies 2022

Phys. Chem. Chem. Phys., 2022, **24**, 10044–10052 | **10051**

48 M. Cerón, F. Li and L. Echegoyen, *J. Phys. Org. Chem.*, 2014, **27**, 258–264.

49 J. Biskupek, S. T. Skowron, C. T. Stoppiello, G. A. Rance, S. Alom, K. L. Y. Fung, R. J. Whitby, M. H. Levitt, Q. M. Ramasse, U. Kaiser, E. Besley and A. N. Khlobystov, *ACS Nano*, 2020, **14**, 11178–11189.

50 M. Waiblinger, K. Lips, W. Harneit, A. Weidinger, E. Dietel and A. Hirsch, *Phys. Rev. B: Condens. Matter Mater. Phys.*, 2001, **64**, 159901.

51 B. Pietzak, M. Waiblinger, T. Almeida Murphy, A. Weidinger, M. Höhne, E. Dietel and A. Hirsch, *Chem. Phys. Lett.*, 1997, **279**, 259–263.

52 P. Delaney and J. C. Greer, *Appl. Phys. Lett.*, 2004, **84**, 431–433.

53 S. Lo, A. V. Korol and A. V. Solovyov, *J. Phys. B: At., Mol. Opt. Phys.*, 2007, **40**, 3973–3981.

54 G. Gao and H. S. Kang, *Chem. Phys. Lett.*, 2008, **462**, 72–74.

55 A. V. Marenich, C. J. Cramer and D. G. Truhlar, *Chem. Sci.*, 2013, **4**, 2349–2356.

56 R. R. Zope, S. Bhusal, L. Basurto, T. Baruah and K. Jackson, *J. Chem. Phys.*, 2015, **143**, 084306.

57 S. M. Avdoshenko, *J. Comput. Chem.*, 2018, **39**, 1594–1598.

58 J. A. Luque-Urrutia, A. Poater and M. Solà, *Chem. – Eur. J.*, 2020, **26**, 804–808.

59 H. Zettergren, H. T. Schmidt, P. Reinhed, H. Cederquist, J. Jensen, P. Hvelplund, S. Tomita, B. Manil, J. Rangama and B. A. Huber, *J. Chem. Phys.*, 2007, **126**, 224303.

60 E. B. Lindgren, H.-K. Chan, A. J. Stace and E. Besley, *Phys. Chem. Chem. Phys.*, 2016, **18**, 5883–5895.

61 W. I. F. David, R. M. Ibberson, J. C. Matthewman, K. Prassides, T. J. S. Dennis, J. P. Hare, H. W. Kroto, R. Taylor and D. R. M. Walton, *Nature*, 1991, **353**, 147–149.

62 J. Tao, J. Yang and A. M. Rappe, *J. Chem. Phys.*, 2015, **142**, 164302.

63 T. He, G. Gao, L. Kou, G. Will and A. Du, *J. Catal.*, 2017, **354**, 231–235.

64 X. Chen, H. Zhang and N. Lai, *J. Mater. Sci.*, 2020, **55**, 11382–11390.